

# GC Improving Resolution and Clarity with Neural Networks\*

**Christopher P. Ross<sup>1</sup>**

Search and Discovery Article #41911 (2016)

Posted October 10, 2016

\*Adapted from the Geophysical Corner column, prepared by the author, in AAPG Explorer, September, 2016. Editor of Geophysical Corner is Satinder Chopra ([schopra@arcis.com](mailto:schopra@arcis.com)). Managing Editor of AAPG Explorer is Brian Ervin. AAPG © 2016

<sup>1</sup>Cross Quantitative Interpretation LP, Santa Fe, NM ([cross@crossqi.com](mailto:cross@crossqi.com))

## **General Statement**

Tight sands by their very nature imply lower porosity and higher interval velocity, and therefore may be seismically thin and difficult to resolve in the seismic record. Targeting lower porosity siltstones instead of sandstones can further increase the degree of difficulty. Nevertheless, with improved drilling and development technologies, tight sands and silts are now often exploration and production objectives. Seismic inversion techniques have been used extensively for these problematic, seismically thin reservoirs for decades since the inversion process removes the wavelet through deconvolution or equivalent techniques, allowing interpreters to get closer to resolving the top and base of these units. However, when working with seismic objectives below seismic tuning thicknesses, there are still limitations. Here, I demonstrate with a thin, spatially varying siltstone reservoir how to improve seismic inversion resolution and better clarity of lithologies using mapping and classifying supervised neural networks.

## **Geology**

The setting for this article is the Permian Basin of West Texas, and it focuses on the Woodford group – a relatively thin, predominantly clastic interval of Mississippian and Devonian age strata situated unconformably between Mississippian and Devonian carbonates. Of interest is the Mississippian-age Woodford Silt, unconformably overlying the organic-rich, black Devonian Woodford Shale. The Woodford Shale ranges from 50 to 200 feet in gross thickness across the 3-D survey, while the silt varies in thickness from 40 to 120 feet, and can be subdivided from core analysis into two parts: a less desirable basal section that is a ripple laminated, argillaceous siltstone (shaley); and a more desirable upper portion described as intensely bioturbated to bioturbated coarse siltstone. Porosity ranges for the upper portion of the silt are 2 percent to 8 percent. While differentiating the upper and lower silt facies would be advantageous, the first-order goal is to determine the thickness and extent of the combined facies of silt, which has similar acoustic impedance ranges with the Woodford Shale. This task is further complicated by significant contrast in impedances with the encasing carbonates.

## Seismic Data and Inversion

The Woodford Silt has a tuning thickness of 127 feet, which is larger than the average silt thickness of 80 feet within the 120 square-mile 3-D survey. Thus the Woodford Silt is below tuning, and attempts to measure the thickness of the silt will be challenging and complicated by the underlying shale, which has similar impedance ranges. In these thin reservoir settings, seismic inversion technology is routinely considered and there are numerous inversion methodologies available to geoscientists. I will discuss and demonstrate results from a prestack inversion variety known as full waveform inversion (FWI), and another known as probabilistic neural network inversion (PNN), which is a post-stack inversion.

FWI is a progressive, prestack modelbased process that minimizes the errors between the observed prestack record and the synthetic prestack record by perturbing and constraining the elastic and anisotropic model parameters simultaneously with wave-equation modeling. Well logs may be used as part of the low-frequency initial model building, but are not used directly for the iterative error minimization. Acoustic impedance ( $Z_p$ ), shear impedance ( $Z_s$ ), bulk density ( $\rho$ ) and the compressional-to-shear velocity ratio ( $V_p/V_s$ ) are among the typical outputs from an FWI inversion. For this article, the  $Z_p$  seismic component (volume) of the inversion will be used to assess the silt and shale.

PNN is very different from FWI in several ways: it is a post stack approach; uses multiple seismic attributes and it does not deconvolve a wavelet. Rather, the wavelet is effectively removed through the combination of multiple attributes with various weights. PNN directly uses the well data ( $Z_p$  in this case) in an error minimization approach, and constrains the attributes and attribute weighting simultaneously. Furthermore, PNN can be computed at sub-seismic sample rates, which does increase the resolution. This is significantly different from the FWI and convolutional-based inversion approaches that remove the wavelet but do not actually increase the resolution.

## Inversion Comparison

Comparison of the two seismic inversions is achieved by sampling each seismic volume at the control wells within the 3-D. This will permit direct evaluation of the accuracy of the final seismic impedance response with hard data at the wells, and a better understanding of the impedance profiles with regard to silt and shale. [Figure 1a](#) shows the FWI  $Z_p$  inversion and [Figure 1b](#) shows the PNN  $Z_p$  inversion. Higher impedance Devonian and Mississippian carbonates are shaded blue and gray, while the lower impedance clastics are shaded in green, red and yellow. One can recognize the slight shifts in seismic  $Z_p$  curves (red) with the well log  $Z_p$  curves owing to time-depth factors in this depth cross-section. However, for the majority of the wells, these are relatively minor shifts and the comparison of seismic inversion accuracy to well data is straightforward.

Overall the FWI inversion follows the low impedance changes observed by the well logs. The FWI  $Z_p$  inversion also identifies the thicker carbonate units fairly well. All the same, the thinner clastic intervals, while recognized by the FWI inversion, do not exhibit the same dynamic range (hitting the minimum  $Z_p$  accurately); are broader than the actual formation thickness (apparent thickness); and show artifacts on either side of the interval as the FWI is unable to sample the relative impedance change (high-to-low and low-to-high) sufficiently.

With the exception of Well E (track 9, located on the southern-most edge of the survey), which is problematic for both inversions, much better adherence to the well data is observed in [Figure 1b](#), where the neural network  $Z_p$  inversion follows more accurately the thicker carbonate strata,

and better approximates the lower impedance clastic unit's thicknesses. Since it was computed at half of the sample rate of the FWI, it is higher resolution, and the aforementioned comments reflect that. Nine seismic attributes were weighted and combined in a non-linear manner to create this  $Z_p$  curve, and several of the attributes were from the FWI inversion. The PNN  $Z_p$  inversion can be thought of as a higher order  $Z_p$ , and the FWI can be considered as a very good first order approximation. Note that similar PNN  $Z_p$  answers can be obtained without including the FWI attributes as input.

Reviewing the Mississippian carbonate to Woodford Silt to Woodford Shale impedance profiles in Wells F, A, H, I and B (labeled tracks 4, 5, 6, 7 and 8, respectively, at the base of each well), one observes the higher carbonate  $Z_p$  to a lower silt  $Z_p$ , overlying a relatively lower shale  $Z_p$ . However, Wells C and D (tracks 10 and 3) show that silts can sometimes have equivalent  $Z_p$  or slightly greater  $Z_p$  than the overlying silt, which can be problematic for those trusting in a “ $Z_p$ only” methodology to map out silts and shales. Moreover, looking at these nine wells, one can see that silt impedance varies from well to well just as the shales do – indicating a variable response across the area that will make it difficult to use a specific  $Z_p$  color key that reflects solely the occurrence of silt or shale. To remedy this, seismic object detection is used to classify the silts, shales and carbonates.

### Seismic Facies Classification

The neural network classification scheme used in this example is a supervised multilayer perceptron (MLP). This is different from an unsupervised Kohonen self-organizing map (KSOM) or unsupervised vector quantizer (UVQ) methodology in two ways: first, it is supervised and therefore exploits the well data to score the quality of the output; and second, it can address non-linear problems that KSOM and UVQ cannot. In essence, the process will map multiple input seismic attributes ( $Z_p$  included) to a reduced set of output attributes. Here “map” means to “combine and weight” the different seismic attributes to a seismic facies classification volume. For this geological setting, the data will be classified into four seismic facies: Mississippian Carbonate; Woodford Silt; Woodford Shale and Devonian Carbonate. Well data is used to train the seismic attributes to yield a seismic facies log at each CDP. This is the supervised portion of the process, or the feedback that allows the computations to map the attributes to classified seismic facies.

[Figure 2](#) presents the seismic object detection classification in the same manner as the  $Z_p$  inversions in [Figure 1](#), by sampling the seismic volumes at the wells. In [Figure 2a](#), seismic class is presented as the variable area color-filled log, and well log  $Z_p$  as the blue curve in each well track. The well  $Z_p$  is overlain to demonstrate the variability of silt and shale impedance and how the multi-attribute classification approach better captures these variabilities, or, seeing how the MLP algorithm generalizes the variability of the silt, shale and limestone  $Z_p$ . Neural networks are good generalizers and will map slightly different inputs to a common output. Again, outside of problem Well E, the classification offers an improved seismic volume to extract lithology information, especially in conjunction with the silt relative probability volume.

To go full circle, I have substituted for the  $Z_p$  curve an extracted seismic trace from the full stack volume and superimposed it over the seismic facies classification in [Figure 2b](#). This demonstrates the improved clarity in identifying the silt using the MLP classification, as opposed to using a “seismic-only,” or an “impedanceonly” approach. In spite of the seismic amplitude and character differences, well-to-well, the seismic object detection is systematic and better defines the occurrence of silt and shale that matches the petrophysical divisions supplied by the operational petrophysicist and geologist.

Another way to demonstrate the success of this supervised neural network implementation is to view velocity-density crossplots and colorcode the plots with  $Z_p$ , seismic class and probability of silt (from the MLP). The data plotted is from the top of the Mississippian to about 150 feet below the base of the Woodford Shale. In [Figure 3a](#), the plot is color-coded by well log impedance which, as expected, places all of the carbonates in the upper-right (high impedance) portion of the crossplot. [Figure 1b](#) is the PNN  $Z_p$  which diverges from the ideal presented in [Figure 3a](#) (i.e., the seismic inversion data does not show the clear divisions between the different lithologies that the well data  $Z_p$  shows). While this is very typical of seismic data, it makes the classification effort a non-linear one. To that end, [Figure 1c](#) shows the same crossplot with the seismic classification posted for each sample. For this display, the carbonates are colored in light green and gray, shales in blue, and the prospective silt reservoir in orange, matching the display colors in [Figure 2](#). Examination of this crossplot shows the overlap in sonic and density between the shale and silts, further illustrating a need for a non-linear classification approach. [Figure 3d](#) shows the samples with a relative probability of silt greater than 0.65, color-coded by relative silt probability. [Figure 3](#), clearly validates the multi-attribute classification benefits above a  $Z_p$ -only interpretation.

Horizon slices for the equivalent Woodford silt interval are presented in [Figure 4](#). [Figure 4a](#) is the median extraction of the FWI  $Z_p$  and [Figure 4b](#) is the median extraction of the relative silt probability with a transparency applied to all probabilities less than 0.65. In [Figure 4a](#), the red and yellow colors correspond to silt (and some shale) impedance ranges, but one cannot be certain that these ranges are appropriate across the entire 3-D. In contrast, [Figure 4b](#) portrays the occurrence of silt more succinctly by the extraction of higher relative probabilities of Woodford Silt; thus one is not really concerned with the color range of silt or shale, but rather the effective silt relative probability cutoff – a better concern to contemplate.

## Conclusions

Using supervised neural networks for mapping reservoir properties can improve resolution as demonstrated by the PNN  $Z_p$  inversion, or using such networks for classifying variable lithologies can improve clarity as established by the seismic object detection result. While seismic inversion methodologies should be standard operating procedures for these more difficult geological settings, results can be ameliorated using non-linear neural network approaches that incorporate the inversion outputs and or use alternative multiple attributes. The results presented here reflect the neural network capabilities for tight sandstone or silt reservoirs, and how they can impact exploration and development decisions. These same approaches can be applied to unconventional resource plays as well, using mapping and classification techniques for reservoir parameters.

## Acknowledgements

Thanks to Schlumberger for permission to present the seismic data, and thanks to Charlie Mims for his review and comments.



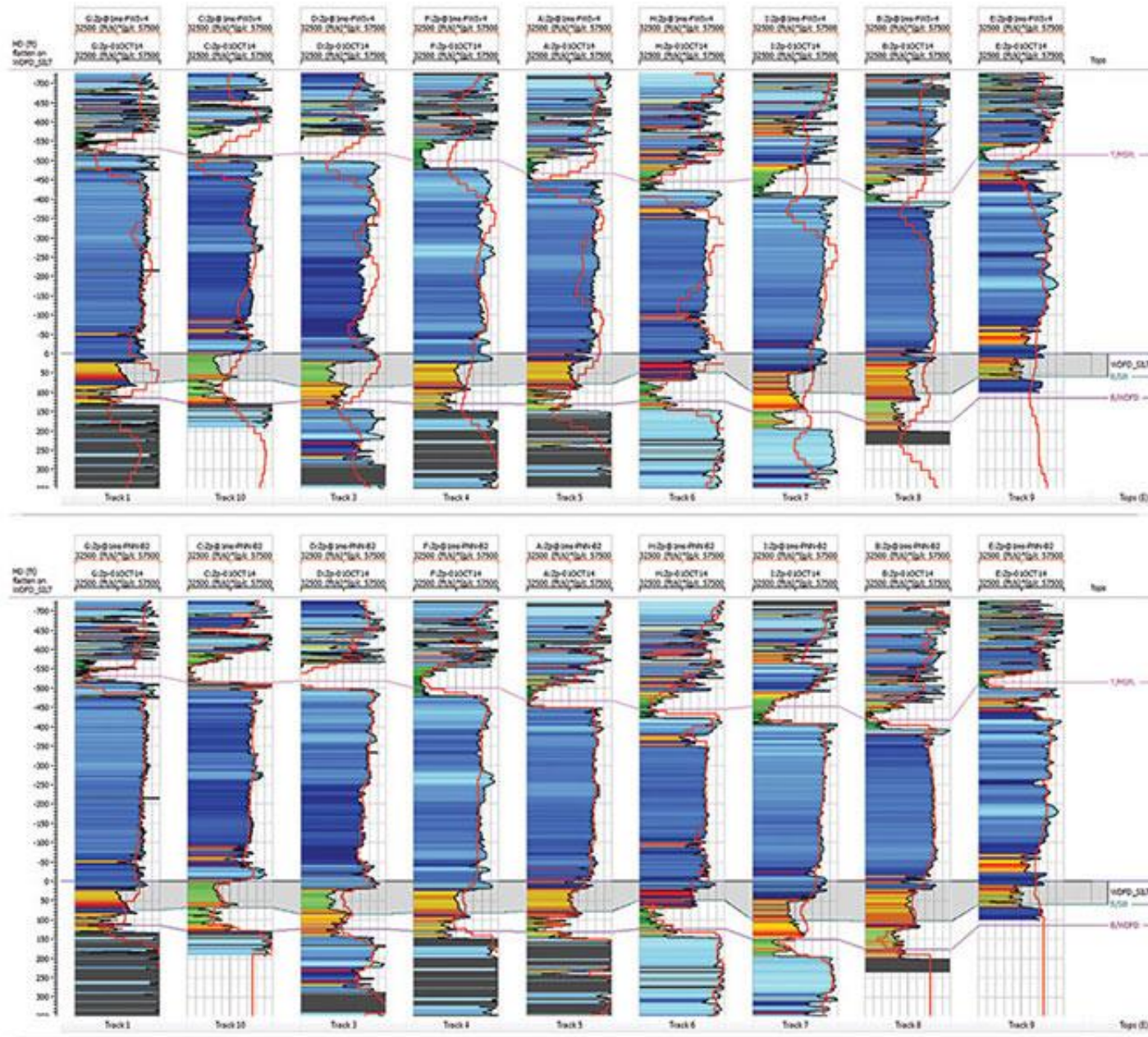


Figure 1. (a) FWI, and (b) PNN.  $Z_p$  inversion at wells.

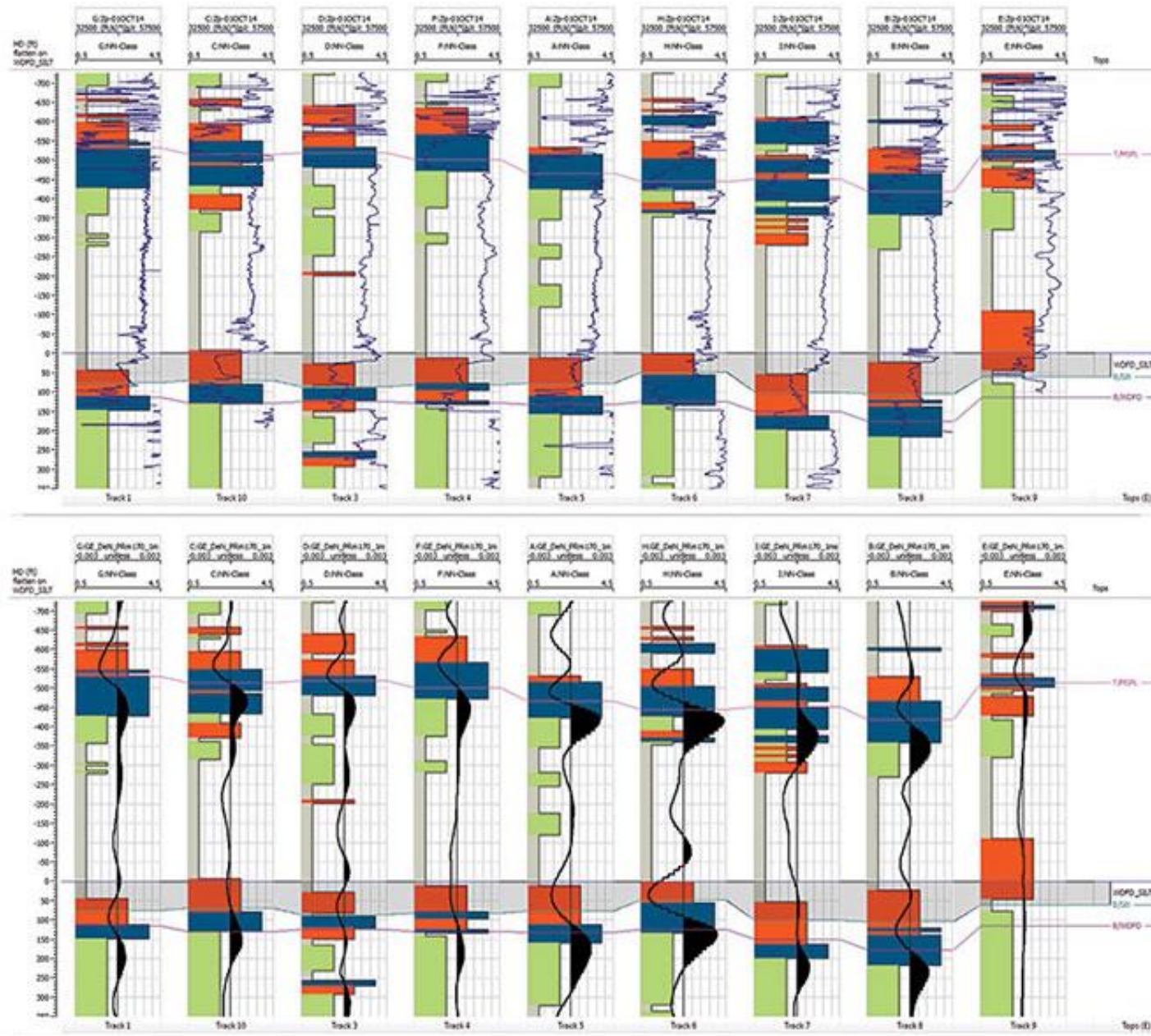
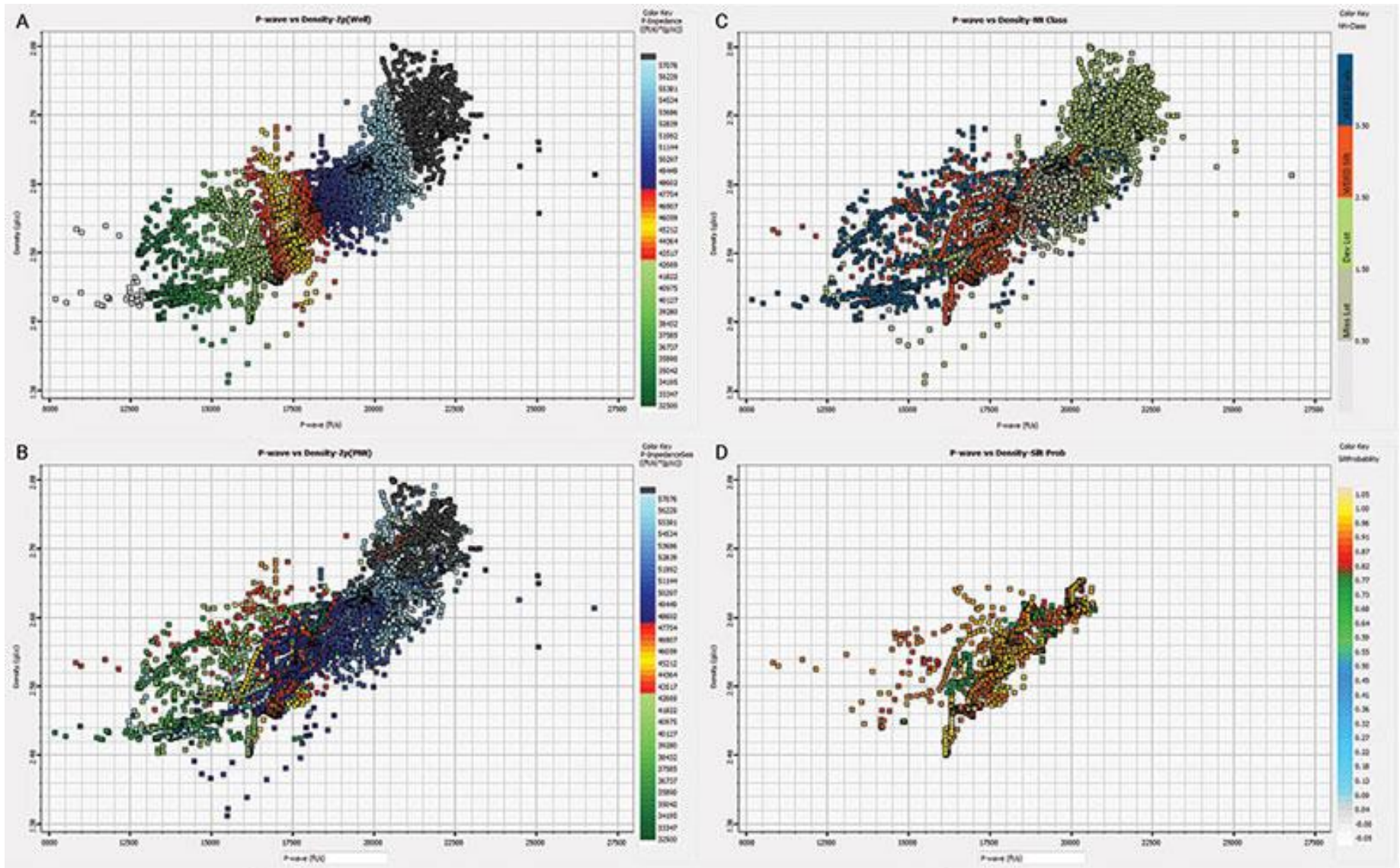


Figure 2. (a) Well Zp, and (b) Seismic. With classified seismic facies.





Figures 3a-d. Velocity-density crossplots with Zp, seismic class and silt probability.

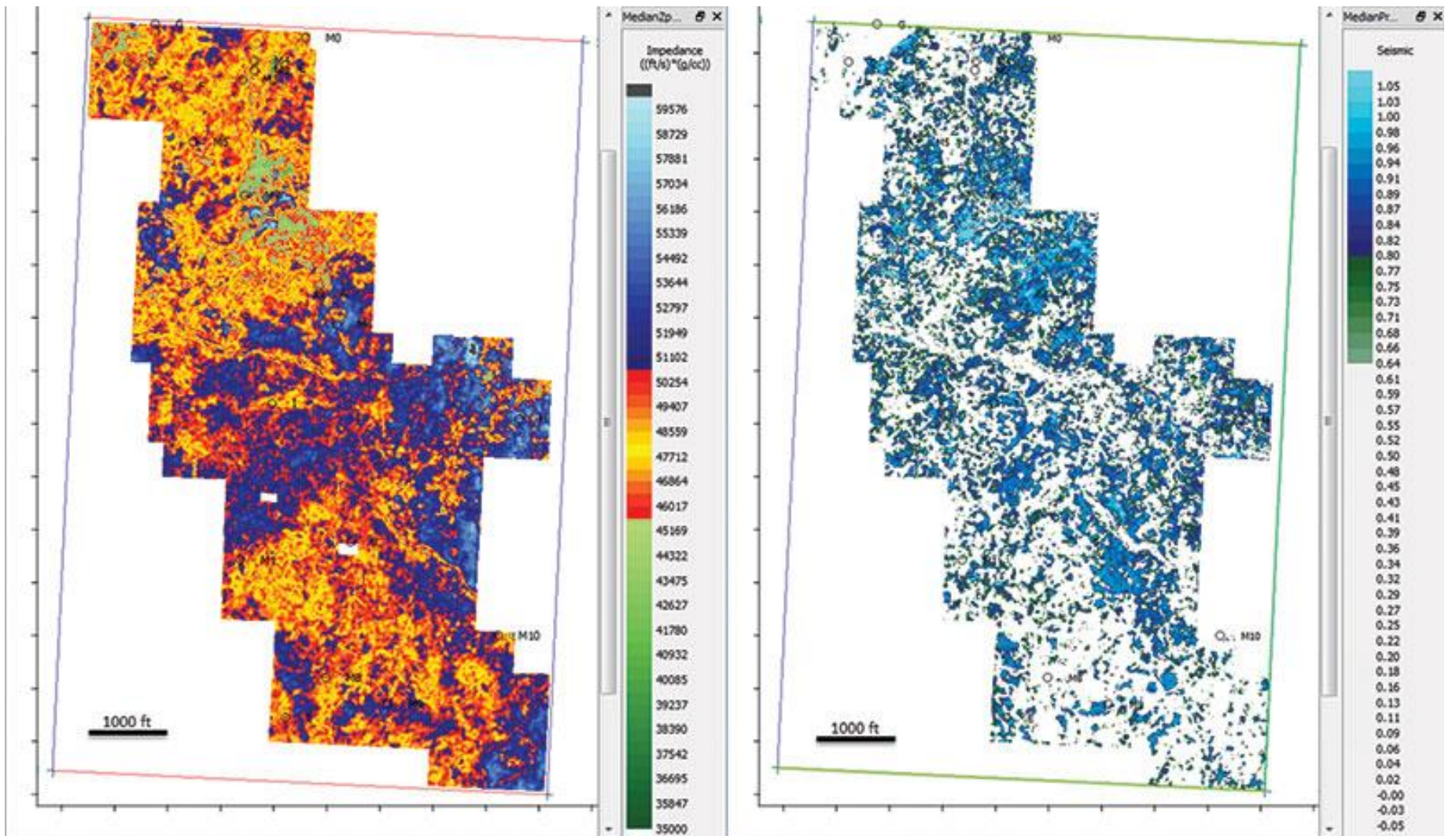


Figure 4. (a) FWI Zp, and (b) Silt probability, horizon slice.